ADVANCED MATERIALS INTERFACES
Open Access
www.advmatinterfaces.de

Correlation of Work Function and Conformation of C_{80} Endofullerenes on *h*-BN/Ni(111)

*Roland Stania, Ari Paavo Seitsonen, Hyunjin Jung, David Kunhardt, Alexey A. Popov, Matthias Muntwiler, and Thomas Greber**

Change of conformation or polarization of molecules is an expression of their functionality. If the two correlate, electric fields can change the conformation. In the case of endofullerene single-molecule magnets the conformation is linked to an electric and a magnetic dipole moment, and therefore magnetoelectric effects are envisoned. The interface system of one monolayer $Sc_2TbN@C_{80}$ on hexagonal boron nitride (h-BN) on Ni(111) has been studied. The molecular layer is hexagonally close packedbut incommensurate. With photoemission the polarization and the conformation of the molecules are addressed by the work function and angular intensity distributions. Valence band photoemission (ARPES) shows a temperature-induced energy shift of the C_{80} molecular orbitals that is parallel to a change in work function of 0.25 eV without charging the molecules. ARPES indicates a modification in molecular conformations between 30 and 300 K. This order–disorder transition involves a polarization change in the interface and is centered at 125 K as observed with high-resolution X-ray photoelectron spectroscopy (XPS). The temperature dependence is described with a thermodynamic model that accounts for disordering with an excitation energy of 74 meV into a high entropy ensemble. All experimental results are supported by density functional theory (DFT).

1. Introduction

Fullerenes are archetypal molecular building blocks in nanoscience. Correspondingly, carbon shells like C_{60} have been studied in detail on surfaces.[1–3] Like found in 3D[4] the freezing of rotational degrees of freedom also causes phase transitions in 2D systems.[5–7] A peculiar phase transition of a monolayer of C_{60} on a single layer of *h*-BN on Ni(111) showed a temperature dependent charge transfer onto C_{60} that is triggered by a change in conformation of the molecules with respect to the substrate.[8]

Endohedral fullerenes are carbon cages that contain atoms.[9] Species with a similar robustness as C_{60}[10] open more opportunities for the exploitation of molecular functionality, such as single molecule magnetism.[11] The first surface science experiments focused on the electronic properties of multilayer C_{80} endofullerenes,[12,13] and soon monolayer systems were prepared and observed with scanning probes.[14–17] At low temperatures, the orientation of the endohedral unit is not random[15] and is related to the magnetization.[17–19] The orientation of the endohedral units may even be changed by magnetic fields.[20] On the other hand, the incomplete screening of the anisotropic electrostatic potential of the endohedral cluster[21] bears a handle for accessing the magnetization of the endohedral clusters with electric fields.

Here we report on a phase transition of a 2D interface system consisting of one monolayer $Sc_2TbN@C_{80}$ on *h*-BN/Ni(111) centered at 125 K. *h*-BN/Ni(111)[22] takes the role of a weakly bonding substrate leaving the adsorbates many degrees of freedom.[23] The phase transition is visible as a change in work function that is considered to reflect the order parameter and is accompanied with a modification in molecular conformation which is seen in a disappearance of the angular dependence of the photoemission from C_{80} molecular orbitals. A temperature induced

R. Stania, T. Greber
Physik-Institut
Universität Zürich
Zürich CH-8057, Switzerland
E-mail: greber@physik.uzh.ch

The ORCID identification number(s) for the author(s) of this article can be found under https://doi.org/10.1002/admi.202300935

DOI: 10.1002/admi.202300935

R. Stania, H. Jung
Center for Artificial Low Dimensional Electronic Systems
Institute for Basic Science
Pohang KR-37673, South Korea

A. P. Seitsonen
Département de Chimie
École Normale Supérieure
Paris F-75005, France

D. Kunhardt, A. A. Popov
Leibniz Institute of Solid State and Materials Research
D-01069 Dresden, Germany

M. Muntwiler
Photon Science Division
Paul Scherrer Institut
Villigen PSI CH-5232, Switzerland

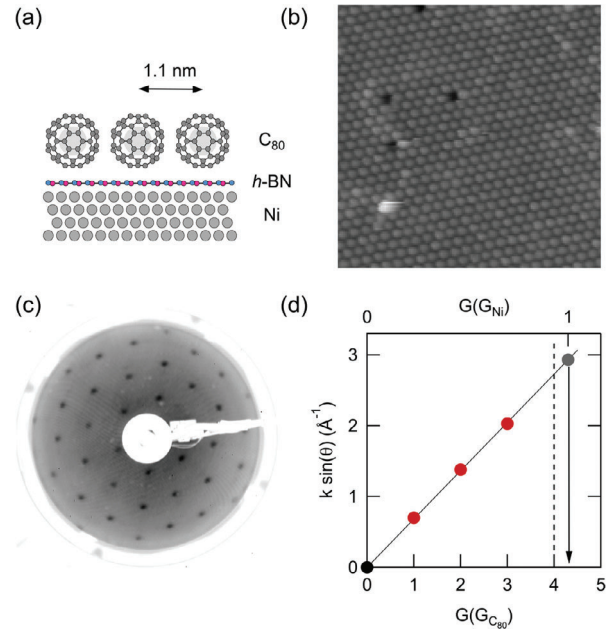

Figure 1. $Sc_2TbN@C_{80}$ on *h*-BN/Ni(111). a) Sketch. b) STM image of a monolayer preparation recorded at 77 K. (Area = 25 × 25 nm^2, I_t= 1 nA, V_t= −5 mV). c) LEED pattern (E = 30 eV) recorded at room temperature. An ordered C_{80} (1 × 1) structure with a lattice constant of 1.09 ± 0.05 nm is discerned. d) Parallel component of the LEED scattering vector of $Sc_2TbN@C_{80}$ from panel (c) (red) and *h*-BN/Ni(111) (gray) from Figure S1, Supporting Information, versus reciprocal lattice vectors G_{Ni} and $G_{C_{80}}$. The C_{80} and the Ni lattices are aligned and incommensurate, where one C_{80} fits on ≈4.3 × 4.3 substrate unit cells.

change of work function was also observed in the case of C_{60} on *h*-BN/Ni(111).[8] Changes in work function indicate a modification in the surface dipole and the related electrical fields. In the present case we find no charge transfer onto the molecule but polarisation of the interface between C_{80} and *h*-BN.

2. Results and Discussion

Figure 1 depicts the investigated 2D interface system: A monolayer of $Sc_2TbN@C_{80}$ on *h*-BN/Ni(111), with low temperature scanning tunneling microscopy (STM) and room temperature low energy electron diffraction (LEED) experiments. The STM image shows hexagonally close packed molecules with a lattice constant of ≈1.1 nm, and LEED indicates large scale ordering along the high symmetry directions of the substrate. While C_{60} on *h*-BN/Ni(111) forms a commensurate Ni (4 × 4) superstructure,[8] the C_{80} molecules are about a factor of $\sqrt{80/60} = 1.15$ larger and thus may not accommodate in 4 × 4 Ni(111) unit cells. For the present case the analysis of the LEED spot positions in Figure 1 indicates an aligned but incommensurate ≈4.3 × 4.3 super structure of $Sc_2TbN@C_{80}$ on *h*-BN/Ni(111). In the following we refer this structure as C_{80} (1 × 1). The alignment of the molecular lattice with that of the substrate and the relative lattice constant are inferred from the LEED pattern in Figure 1c and Figure S1, Supporting Information. The C_{80} lattice constant and a low lateral energy landscape corrugation for an incommensurate structure is confirmed by DFT (see Supporting Information), while the orientation of the incommensurate molecular lattice is likely guided by atomic steps in the substrate that run along high symmetry ⟨1$\bar{1}$0⟩ directions, as it was found for $Dy_3N@C_{80}$ on Cu(111).[15]

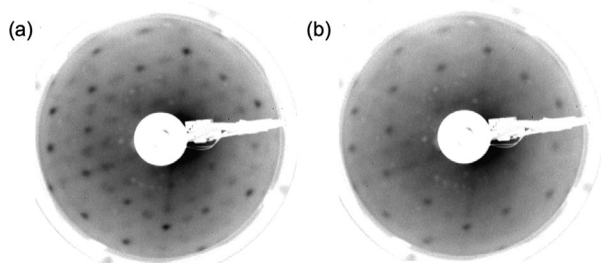

Figure 2. LEED (E = 26.4 eV) from $Sc_2TbN@C_{80}$ on *h*-BN/Ni(111) at two different temperatures. a) C_{80} (2 × 2) phase at 83 K. b) At 170 K the C_{80} (1 × 1) phase dominates as at room temperature (see Figure 1c).

Figure 2 shows the formation of a C_{80} (2 × 2) low temperature superstructure in the incommensurate monolayer of $Sc_2TbN@C_{80}$ on *h*-BN/Ni(111). The structure forms between 80 and 170 K. Such low temperature ordering or freezing of fullerenes is known from C_{60} films, where below 100 K a C_{60} (2 × 2) structure was established[5,6] and for C_{60} on *h*-BN/Ni(111) a $(\sqrt{3} \times \sqrt{3})$ phase was found below 160 K.[8] This indicates that like in 3D,[4] intermolecular forces lead to ordering of the fullerenes below room temperature in 2D systems. The interaction between $Sc_2TbN@C_{80}$ molecules is, however, expected to be more involved than that between C_{60} because the icosahedral symmetry of the C_{80} cage is broken by the endohedral unit, which is reflected in their appearance as ellipsoids that are weakly distorted from spherical shape, and their permanent dipole moments (see Supporting Information).

The experimental proof for molecular order below 100 K provided angular resolved photoelectron spectroscopy (ARPES). **Figure** 3 displays He Iα excited valence band photoemission data

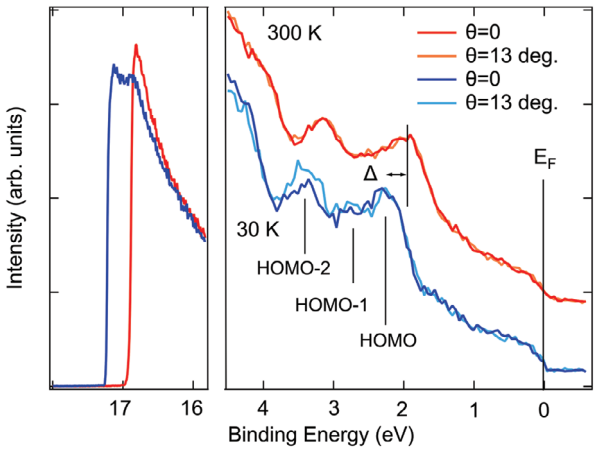

Figure 3. Angular resolved He Iα excited valence band photoemission from $Sc_2TbN@C_{80}$ on *h*-BN/Ni(111). The temperature induced shift Δ = 0.26 ± 0.02 eV of the molecular orbital-peaks labeled as HOMO, HOMO-1, and HOMO-2 is parallel to the shift of the secondary electron cut off (left panel) that indicates a work function increase from 3.95 eV at 30 K to 4.20 eV at 300 K. At low temperature the molecular orbitals display anisotropy with polar emission angle θ, while at room temperature they do not.

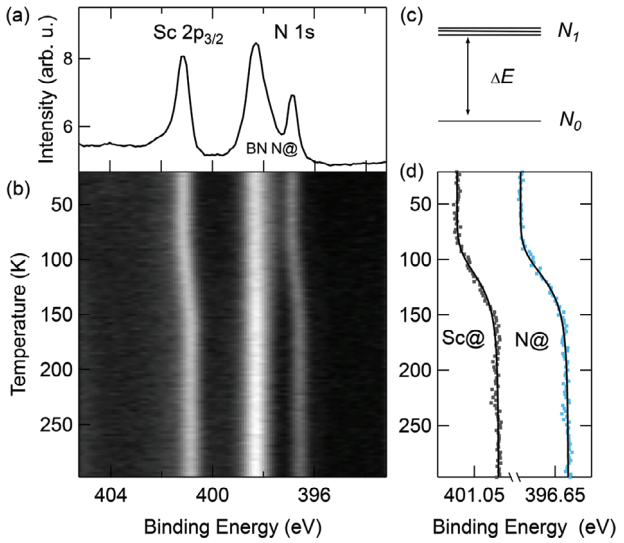

Figure 4. XPS from $Sc_2TbN@C_{80}$ on *h*-BN/Ni(111) (photon energy $h\nu = 600$ eV). a) Spectrum in the binding energy range of the N 1s and the Sc $2p_{3/2}$ core levels. At low temperature the endohedral nitrogen species has a 1.42 eV lower binding energy than the nitrogen of *h*-BN. b) Temperature dependent XPS between 30 and 300 K. c) Two level model for the temperature dependence of the molecular core level energy shifts. The excitation energy ΔE and the degeneracy N_1 are the only thermodynamic parameters. d) Endohedral Sc $2p_{3/2}$ (gray) and N 1s (light blue) binding energies as a function of the sample temperature with a fit of the two level model—solid lines.

and the corresponding secondary electron cutoff of $Sc_2TbN@C_{80}$ on *h*-BN/Ni(111) at 30 and 300 K. The work function increases with temperature from 3.95 to 4.20 eV. As the highest occupied molecular orbitals (HOMO's) shift in the same direction and by the same amount as the secondary cut off, this indicates vacuum level alignment of the $Sc_2TbN@C_{80}$ molecular orbitals, which is expected for a weak bonding to the substrate.[22] Notably, the work function shift has the same temperature trend for C_{60}/*h*-BN/Ni(111),[8] but in the present case, it is twice as strong and it is not related to a charge transfer that would be reflected in an onset of occupation of the lowest unoccupied molecular orbital (LUMO). The HOMO peak of $Sc_2TbN@C_{80}$ on *h*-BN/Ni(111) occurs at relatively high binding energies of 2.30 and 2.04 eV at 30 and 300 K. They are larger than the optical gap of $Sc_2YN@C_{80}$ in toluene of 1.72 eV[24] and indicative for a strong on site Coulomb interaction U.[1,25] In multilayer $Sc_3N@C_{80}$ the HOMO was found at ≈1.73 eV binding energy.[12] The valence band data show significant angular anisotropy of the molecular orbital intensities at low temperature, while it is much smaller at room temperature. Such intensity variations are known as ultraviolet photoelectron diffraction (UPD) effects[26–28] and signal orientational order of the molecules at low temperatures. As the LEED data in Figure 2, this confirms a picture where the conformational order of the C_{80} molecules increases at low temperature and furthermore that this is accompanied with a decrease of the work function.

Figure 4 shows X-ray photoelectron spectroscopy (XPS) of $Sc_2TbN@C_{80}$ on *h*-BN/Ni(111) between 30 K and room temperature. The phase transition is reflected in core levels assigned to the molecular layer with a maximum rate of change that is centered at 125 K. The N 1s and the Sc $3p_{3/2}$ core levels are observed. The N 1s level of the endohedral unit and the *h*-BN substrate are chemically shifted. Relative to the N 1s levels of the *h*-BN substrate they display at lower binding energy, and sharper. This is in perfect agreement with calculated N 1s spectra (see Supporting Information). The N 1s orbitals of the atoms in the molecules follow the work function, that is show the same energy shift as the secondary cut off and the HOMO molecular orbitals in Figure 3 while the *h*-BN N 1s orbitals of the substrate have constant binding energy. This means that the *h*-BN N 1s energy does not follow the temperature dependence of the vacuum level, while the one of the molecular layer on top of *h*-BN does. Besides the endohedral N 1s and Sc $2p_{3/2}$ also the C 1s carbon cage core levels shift parallel to the work function (see Supporting Information). As no charge is transferred into the LUMO, the work function change must be due to polarisation of the molecular layer and the *h*-BN. Since all core levels of the molecule shift parallel to the work function, the molecules act as entities with a common dipole moment. The observed behavior of the work function is assigned to the onset of molecular rotation and different resulting dipole components p_z along the surface normal. The work function and dipole component change $\Delta\Phi$ and Δp_z are connected via the Helmholtz equation $\Delta\Phi = -\frac{n e}{\epsilon_0}\Delta p_z$, where n is the areal density of the dipoles, e is the elementary charge, and ϵ_0 is the vacuum permittivity. Taking the calculated gas phase dipole moment of $Sc_2YN@C_{80}$ of 0.25 D (see Supporting Information) we would get a work function increase of 92 meV with the dipole density n of the C_{80} layer in going from a configuration where the dipole points antiparallel to the surface normal to an isotropic configuration with a zero average dipole moment. Calculations of 120 different conformations of $Sc_2YN@C_{80}$ on $\sqrt{19}$ *h*-BN/Ni(111) show a larger variation than 92 meV. The full width at half maximum (FWHM) of the work function distribution is 190 meV (Figure S7c, Supporting Information), which is closer to the experimentally observed effect of 250 ± 5 meV. This suggests that the polarization response of the *h*-BN interface increases the effect significantly. Reasons for the remaining difference between theory and experiment may be the incommensurability and the (2 × 2) molecular ordering at low temperature.

The temperature dependence of the core level binding energies is parallel to the work function. This allows to extract thermodynamic properties of the $Sc_2TbN@C_{80}$ on *h*-BN/Ni(111) phase transition. As seen in Figure 3, at higher temperature more molecular conformations are populated because there is no angular anisotropy of the molecular orbitals observed. This does not lead to an important broadening of the spectra, because the bonding of the molecules is relatively weak, and the energy reference is the vacuum level. Therefore, the core level binding energy shifts reflect the global order parameter or work function as a measure for molecular arrangement. To model we consider for the molecular conformations two energy levels that are separated by an excitation energy $\Delta E = E_1 - E_0$. As the experiment is not sensitive to the absolute degeneracy N_0 is set = 1 and the degeneracy of E_1 is N_1 (see Figure 4c). From the calculations (see Supporting Information) it is seen that the assumption of two conformational energies is a simplification, though the data in Figure 4d do not allow for the reliable

fitting of more than four independent parameters. At thermal equilibrium we obtain the occupation $\langle n_0 \rangle$ of the lowest energy state E_0,

$$\langle n_0 \rangle = \frac{1}{1 + N_1 \exp\left(-\Delta E / k_B T\right)} \quad (1)$$

and the occupation of state E_1, $\langle n_1 \rangle = 1 - \langle n_0 \rangle$. The measured core level binding energies $E_B(T)$ are taken to express the order parameter that is, the weighted sum $E_B = \langle n_0 \rangle E_{B0} + \langle n_1 \rangle E_{B1}$.

E_{B0} describes the system at $T = 0$ or $\langle n_1 \rangle = 0$ and E_{B1} is the core level energy if all molecules were excited, that is, $\langle n_1 \rangle = 1$. From $E_B(T)$ the thermodynamic model parameters ΔE and N_1 are determined. The solid lines in Figure 4d show the fits of the N_1 degenerate two level model for the N 1s and the Sc $2p_{3/2}$ core levels. The parameters from both fits are $\Delta E = 74 \pm 6$ meV, $E_{B0} - E_{B1} = 310 \pm 40$ meV and $N_1 = 1300 \pm 700$ for the degeneracy of E_1. The excitation energy ΔE has the order of magnitude of the standard deviation of the calculated conformations (68 meV; see Supporting Information). This means that the excitation energy in the phase transition has the energy scale of different molecular conformations of $Sc_2YN@C_{80}$/*h*-BN/Ni(111). $E_{B0} - E_{B1}$ is in line with the work function shift and confirms that the observed work function shift is about three times larger than what would be expected from the molecular dipole moment in the gas phase. This emphasizes the importance of the interface if a large effect shall be obtained. The degeneracy N_1 reflects the large C_{80} (2×2) unit cell at low temperature and points to a strong contribution of the entropy to the free energy of the system above the ordering temperature.

3. Conclusion

In conclusion, we observed a temperature induced work function shift of $Sc_2TbN@C_{80}$ on *h*-BN/Ni(111) centered at 125 K. This shift is related to the disappearance of a $Sc_2TbN@C_{80}$ (2×2) LEED structure. The transition is an order disorder transition with onset of rotation of the endohedral clusters. DFT calculations, figure out the lattice constant of $Sc_2YN@C_{80}$, a permanent dipole moment, describe the N 1s XPS spectrum in the $\sqrt{19}$ $Sc_2YN@C_{80}$ (1×1) phase and propose different conformers with an energy distribution that is in line with the model for the temperature dependence of the molecular core level binding energies. With these findings we put forward the converse effect i.e. that the molecular orientation may be controlled with an electric field as found in the surface dipole. This would allow the magnetism of endohedral units to be remotely controlled with electric fields, and a magnetoelectric system would become available.

4. Experimental Section

Experimental: $Sc_2TbN@C_{80}$ molecules with icosahedral I_h symmetry of the carbon cage were synthetized and purified as described in ref. [29] and sublimated onto *h*-BN/Ni(111),[22,30] with the substrate kept at 470 K. In order to handle the small quantities of available molecules LoTnE, a home built low temperature nanogram evaporator with small copper Knudsen cells that can be approached close to the sample was used. The photoemission data were recorded at a photon energy of 600 eV or He Iα (21.2 eV).[31] The coverage was determined with a layer by layer growth model, with an electron mean free path of 1 nm and from the intensity ratio of the N 1s core levels of the molecule and *h*-BN.[21] The low energy electron diffraction (LEED) patterns were calibrated with the (0,1) spots of the *h*-BN/Ni(111) substrate (see Supporting Information). Scanning tunneling microscopy (STM) images were recorded at liquid nitrogen temperature.[31]

Theory: Density functional theory (DFT) calculations were performed on the $Sc_2YN@C_{80}$ endofullerene because it is chemically very similar to $Sc_2TbN@C_{80}$ but easier to treat accurately.[21] The incommensurate system was simulated with a *h*-BN/Ni(111)-$(\sqrt{19} \times \sqrt{19})$R23° substrate unit cell that accommodated one molecule. This structure was abbreviated as $\sqrt{19}$. More details are given in the Supporting Information.

Supporting Information

Supporting Information is available from the Wiley Online Library or from the author.

Acknowledgements

The present work was supported by the Swiss National Science Foundation grant Nos.153312 and 201086 and the Institute for Basic Science (IBS-R014-D1). Calculations were performed at the CSCS Swiss National Supercomputing Centre under project uzh11. The photoemission, LEED, and STM measurements were performed at the PEARL beamline of the Swiss Light Source, Paul Scherrer Institut, Villigen. A.A.P. acknowledges Deutsche Forschungsgemeinschaft (grant PO 1602/8-1).

Conflict of Interest

The authors declare no conflict of interest.

Data Availability Statement

The data that support the findings of this study are available from the corresponding author upon reasonable request.

Keywords

endofullerenes on surfaces, order–disorder transition, work function

Received: November 8, 2023
Revised: December 21, 2023
Published online: January 11, 2024

[1] P. Rudolf, M. S. Golden, P. A. Brühwiler, *J. Electron Spectrosc. Relat. Phenom.* **1999**, *100*, 409.
[2] L. Sánchez, R. Otero, J. M. Gallego, R. Miranda, N. Martin, *Chem. Rev.* **2009**, *109*, 2081.
[3] P. J. Moriarty, *Surf. Sci. Rep.* **2010**, *65*, 175.
[4] P. A. Heiney, J. E. Fischer, A. R. McGhie, W. J. Romanow, A. M. Denenstein, J. P. McCauley Jr, A. B. Smith, D. E. Cox, *Phys. Rev. Lett.* **1991**, *66*, 2911.
[5] P. J. Benning, F. Stepniak, J. H. Weaver, *Phys. Rev. B* **1993**, *48*, 9086.
[6] A. Goldoni, C. Cepek, S. Modesti, *Phys. Rev. B* **1996**, *54*, 2890.
[7] A. Goldoni, C. Cepek, R. Larciprete, L. Sangaletti, S. Pagliara, G. Paolucci, M. Sancrotti, *Phys. Rev. Lett.* **2002**, *88*, 196102.

[8] M. Muntwiler, W. Auwärter, A. Seitsonen, J. Osterwalder, T. Greber, *Phys. Rev. B* **2005**, *71*, 121402.
[9] A. A. Popov, S. Yang, L. Dunsch, *Chem. Rev.* **2013**, *113*, 5989.
[10] S. Stevenson, G. Rice, T. Glass, K. Harich, F. Cromer, M. R. Jordan, J. Craft, E. Hadju, R. Bible, M. M. Olmstead, K. Maitra, A. J. Fisher, A. L. Balch, H. C. Dorn, *Nature* **1999**, *401*, 55.
[11] R. Westerström, J. Dreiser, C. Piamonteze, M. Muntwiler, S. Weyeneth, H. Brune, S. Rusponi, F. Nolting, A. Popov, S. Yang, L. Dunsch, T. Greber, *J. Am. Chem. Soc.* **2012**, *134*, 9840.
[12] L. Alvarez, T. Pichler, P. Georgi, T. Schwieger, H. Peisert, L. Dunsch, Z. Hu, M. Knupfer, J. Fink, P. Bressler, M. Mast, M. S. Golden, *Phys. Rev. B* **2002**, *66*, 035107.
[13] H. Shiozawa, H. Rauf, T. Pichler, D. Grimm, X. Liu, M. Knupfer, M. Kalbac, S. Yang, L. Dunsch, B. Büchner, D. Batchelor, *Phys. Rev. B* **2005**, *72*, 195409.
[14] D. F. Leigh, C. Norenberg, D. Cattaneo, J. H. G. Owen, K. Porfyrakis, A. L. Bassi, A. Ardavan, G. A. D. Briggs, *Surf. Sci.* **2007**, *601*, 2750.
[15] M. Treier, P. Ruffieux, R. Fasel, F. Nolting, S. Yang, L. Dunsch, T. Greber, *Phys. Rev. B* **2009**, *80*, 081403.
[16] T. Huang, J. Zhao, M. Peng, A. A. Popov, S. Yang, L. Dunsch, H. Petek, *Nano Lett.* **2011**, *11*, 5327.
[17] D. S. Krylov, S. Schimmel, V. Dubrovin, F. Liu, T. T. Nhung Nguyen, L. Spree, C. Chen, G. Velkos, C. Bulbucan, R. Westerström, M. Studniarek, J. Dreiser, C. Hess, B. Büchner, S. M. Avdoshenko, A. A. Popov, *Angew. Chem. Int. Ed.* **2020**, *59*, 5756.
[18] R. Westerström, A.-C. Uldry, R. Stania, J. Dreiser, C. Piamonteze, M. Muntwiler, F. Matsui, S. Rusponi, H. Brune, S. Yang, A. Popov, B. Büchner, B. Delley, T. Greber, *Phys. Rev. Lett.* **2015**, *114*, 087201.
[19] T. Greber, A. P. Seitsonen, A. Hemmi, J. Dreiser, R. Stania, F. Matsui, M. Muntwiler, A. A. Popov, R. Westerström, *Phys. Rev. Mater.* **2019**, *3*, 014409.
[20] A. Kostanyan, R. Westerström, Y. Zhang, D. Kunhardt, R. Stania, B. Büchner, A. A. Popov, T. Greber, *Phys. Rev. Lett.* **2017**, *119*, 237202.
[21] R. Stania, A. P. Seitsonen, D. Kunhardt, B. Büchner, A. A. Popov, M. Muntwiler, T. Greber, *J. Phys. Chem. Lett.* **2018**, *9*, 3586.
[22] A. Nagashima, N. Tejima, Y. Gamou, T. Kawai, C. Oshima, *Phys. Rev. Lett.* **1995**, *75*, 3918.
[23] W. Auwärter, M. Muntwiler, T. Greber, J. Osterwalder, *Surf. Sci.* **2002**, *511*, 379.
[24] N. Chen, L. Z. Fan, K. Tan, Y. Q. Wuand, C. Y. Shu, X. Lu, C. R. Wang, *J. Phys. Chem. C* **2007**, *111*, 11823.
[25] R. W. Lof, M. A. van Veenendaal, B. Koopmans, H. T. Jonkman, G. A. Sawatzky, *Phys. Rev. Lett.* **1992**, *68*, 3924.
[26] J. Osterwalder, T. Greber, P. Aebi, R. Fasel, L. Schlapbach, *Phys. Rev. B* **1996**, *53*, 10209.
[27] P. Puschnig, S. Berkebile, A. J. Fleming, G. Koller, K. Emtsev, T. Seyller, J. D. Riley, C. Ambrosch-Draxl, F. P. Netzer, M. G. Ramsey, *Science* **2009**, *326*, 702.
[28] M. Greif, L. Castiglioni, A. P. Seitsonen, S. Roth, J. Osterwalder, M. Hengsberger, *Phys. Rev. B* **2013**, *87*, 085429.
[29] Y. Zhang, D. Krylov, M. Rosenkranz, S. Schiemenz, A. A. Popov, *Chem. Sci.* **2015**, *6*, 2328.
[30] W. Auwärter, T. J. Kreutz, T. Greber, J. Osterwalder, *Surf. Sci.* **1999**, *429*, 229.
[31] M. Muntwiler, J. Zhang, R. Stania, F. Matsui, P. Oberta, U. Flechsig, L. Patthey, C. Quitmann, T. Glatzel, R. Widmer, E. Meyer, T. A. Jung, P. Aebi, R. Fasel, T. Greber, *J. Synchrotron Radiat.* **2017**, *24*, 354.